Available online at www.sciencedirect.com

ScienceDirect

Additive Manufacturing 1–4 (2014) 77–86

Additive MANUFACTURING

www.elsevier.com/locate/addma

Reducing porosity in AlSi10Mg parts processed by selective laser melting☆

Nesma T. Aboulkhair[a,*], Nicola M. Everitt[a], Ian Ashcroft[b], Chris Tuck[b]

[a] Materials, Mechanics and Structures Research Division, Faculty of Engineering, University of Nottingham, Nottingham NG7 2RD, United Kingdom
[b] Manufacturing and Process Technologies Research Division, Faculty of Engineering, University of Nottingham, Nottingham NG7 2RD, United Kingdom

Available online 20 August 2014

Abstract

Selective laser melting (SLM) is widely gaining popularity as an alternative manufacturing technique for complex and customized parts. SLM is a near net shape process with minimal post processing machining required dependent upon final application. The fact that SLM produces little waste and enables more optimal designs also raises opportunities for environmental advantages. The use of aluminium (Al) alloys in SLM is still quite limited due to difficulties in processing that result in parts with high degrees of porosity. However, Al alloys are favoured in many high-end applications for their exceptional strength and stiffness to weight ratio meaning that they are extensively used in the automotive and aerospace industries. This study investigates the windows of parameters required to produce high density parts from AlSi10Mg alloy using selective laser melting. A compromise between the different parameters and scan strategies was achieved and used to produce parts achieving a density of 99.8%.

Keywords: Additive manufacturing; Selective laser melting; Al alloys; AlSi10Mg; Porosity; Microstructure

1. Introduction

There is a current need to manufacture geometrically complex structures that are light-weight. Modern industry also has demands for reducing the cost and time of manufacturing. This demand resulted in the development of rapid prototyping. Additive manufacturing (AM) of metallic materials from metallic powder using a laser heat source is often referred to as selective laser melting (SLM) [1–4]. The interest in SLM is partly motivated by the aim of finding a cleaner and more resource efficient manufacturing process. SLM has outstanding ecological indicators since it saves resources as the waste has the potential of approaching zero. Another indicator is eco-design optimization since the technique allows complex parts to be created monolithically, so it allows light weight structuring with a typically 50% weight reduction. In brief, SLM promotes "design for performance" rather than "design for manufacturing" [5].

Selective laser melting can fabricate components from loose powder that can not only have a similar physical shape to conventionally manufactured components but also having similar properties. Moreover, SLM can produce complex parts – that would require a series of manufacturing processes if made by conventional techniques consuming excess material (i.e. waste), time and energy – in one go. In some cases it is even possible to manufacture parts using SLM that cannot be achieved using any conventional manufacturing method [6]. The methodology in SLM is to selectively scan a powder bed and hence melt powder to build the component layer-by-layer [3,4,7,8]. In SLM, components are built on a base plate with a laser beam traversing each layer in the x-y plane. A piston is lowered after each layer to allow deposition of the subsequent layer of powder. The procedure is repeated successively until the part is completed. The time consumed by the SLM process can be divided into primary and auxiliary time. The primary time is that needed for melting the layer of powder, whereas the auxiliary time is for substrate lowering and powder deposition [1,5,7,9].

Aluminium alloys powders are inherently light with poor flowability and high reflectivity along with high thermal conductivity when compared to other SLM candidate materials as shown in Table 1; this means that a high laser power is required

☆ One or more authors of this article are part of the Editorial Board of the journal. Full responsibility for the editorial and peer-review process for this article lies with the journal's Editor-in-Chief Prof. Ryan Wicker and Deputy Editor Prof. Eric MacDonald. Furthermore, the authors of this article had no and do not currently have access to any confidential information related to its peer-review process.

* Corresponding author. Tel.: +44 7539519516.
E-mail addresses: emxntab@nottingham.ac.uk, ntaboulkhair@aucegypt.edu (N.T. Aboulkhair).

http://dx.doi.org/10.1016/j.addma.2014.08.001
2214-8604/

Table 1
Comparing properties of different SLM candidate materials.

SLM candidate material	Flowability (s/50 gm)[a]	Thermal conductivity (W/(m K))	Reflectivity (%)
Ti64	47	6.7 [11]	53–59 [12]
Stainless Steel 316	14.6	21.4 [13]	60 [14]
Al6061	77	172 [13]	91[15]
AlSi10Mg	No flow	146 [13]	91 [15]

[a] Experimental values for flowability are determined using Hall flow rate ASTM standard test method [10]. All powder materials were supplied by LPW Technology, UK.

for melting and to overcome the rapid heat dissipation. Rapid heat dissipation is more common for the solid Al substrate and less common for the Al powder. Moreover, Al alloys are highly susceptible to oxidation, which promotes porosity [2,7]. One of the major challenges in producing Al alloys parts using SLM is minimizing porosity. Several studies have investigated the effect of processing parameters on porosity [5,7,9]. This paper aims to understand the mechanisms of pore formation as an approach towards eliminating them.

The SLM process is controlled by the set of parameters illustrated in Fig. 1 [8]. The major build parameters involved in the process of selective laser melting are scanning speed, hatch spacing, laser power and layer thickness. There are numerous investigations considering these parameters to enhance part density [5,7,9,16]. However, studies on the densification of Al alloys through changing the scanning pattern per layer have yet to be published. Although the effect of scanning strategy on the crystallographic texture of the part, which is expected to influence the material's isotropy, was examined by Thijs et al. [2].

The aim of this paper is to use design of the scanning strategy to enhance the relative density of parts being processed, i.e. minimize the porosity. The importance of manipulating the scanning strategy is that it can be used to amend the defects that are induced during the first scan of the current or preceding layer.

2. Experimental work

AlSi10Mg powder provided by LPW Technology UK were processed to produce test cubes using a Realizer GmbH SLM-50, Germany, equipped with a 100 W yttrium fibre laser (YLM-100-AC). The particle size distribution for the powder was determined using a Malvern UK Mastersizer 3000, which uses laser diffraction to measure the size of particles through measuring the intensity of light scattered as a laser beam passes through a dispersed particulate sample. Data is then analyzed to calculate the size of the particles that created the scattering pattern [17]. A Philips XL30 scanning electron microscope (SEM) with a 20 kV accelerating voltage was used to evaluate powder morphology; in addition the SEM was equipped with an energy dispersive X-ray (EDX) detector that was used for chemical composition analysis. The powder was also cross-sectioned and polished to investigate the presence of inherent pores using a Nikon Eclipse LV100ND microscope. Powder was first dried at 70 °C for 20 min. The SLM process was conducted under an Argon atmosphere with an oxygen level below 0.5%. The test cubes produced were 5 mm × 5 mm × 5 mm. The platform on which the cubes were built was kept at 200 °C to maintain the part at an elevated temperature so as to prevent it from warping due to non-uniform thermal expansion. In order to study the effect of the building parameters on pore creation, the study was divided into the three phases listed below.

2.1. Hatch spacing study

Five sets of samples – each set comprising three samples – were produced using hatch spacing values of 50, 100, 150,

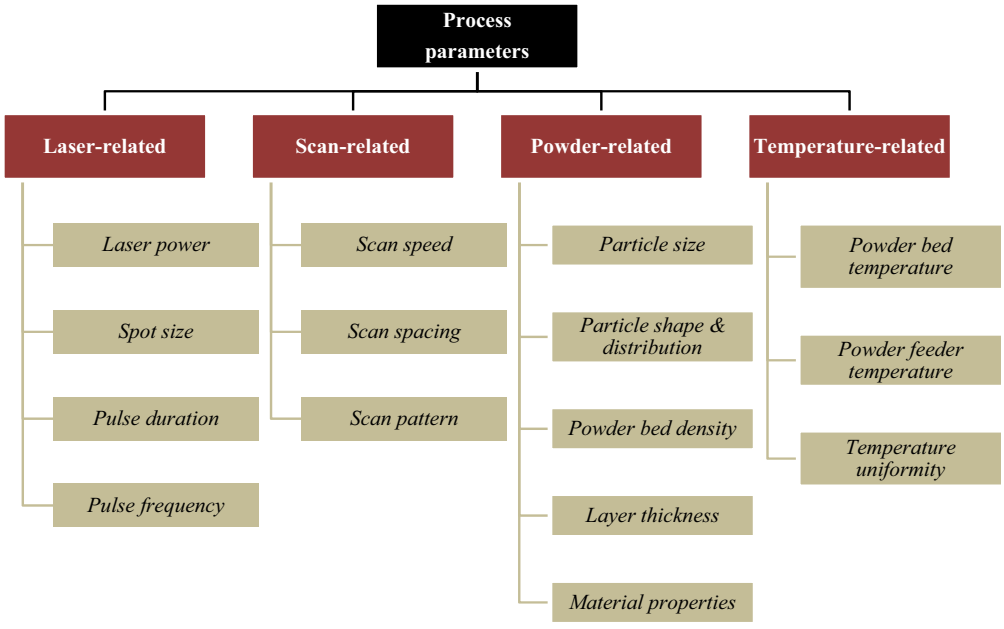

Fig. 1. Controlling parameters in SLM process.

Table 2
Scanning strategies variable parameters.

Scan strategy	No. of scans per layer	Uni or bi-directional	1st scan parameters		2nd scan parameters	
			Power	HS	Power	HS
X	1	Uni	100	50	–	–
2X	2	Uni	100	50	100	50
Alternating	1	Bi	100	50	–	–
X&Y 2HS	2	Bi	100	100	100	50
Pre-sinter	2	Uni	50	50	100	50
Overlap	2	Uni	100	50	100	50

200, and 250 μm. The other parameters were kept constant for all samples in this batch (layer thickness = 40 μm, scanning speed = 500 μm/s, and 100 W laser power). The scanning pattern/orientation in this study was a unidirectional X-axis scan. This was used to simplify the structure of the bulk sample in order to aid in tracing the mechanisms behind the pores and cavity development.

2.2. Scanning speed study

The layer thickness and laser power were kept constant at 40 μm and 100 W, respectively. Scanning speed was varied between 250 and 1000 mm/s with 250 mm/s intervals, along with two different hatch spacings (50 and 100 μm).

2.3. Scan orientation study

The layer thickness was fixed at 40 μm for this study. The samples built were divided into three batches according to the scanning speed used (500, 750, and 1000 mm/s). The scanning strategies investigated for each batch are listed in Table 2. The "X" denotes a unidirectional scan with a single scan per layer. The "2X" is similar to "X" but each layer is scanned twice. The "Alternating" strategy is scanning each layer in a direction rotated by 90° to its precursor. The "X&Y 2HS" indicates that each layer was scanned twice having each scan perpendicular to the one before and with different hatch spacings for each scan. The "Pre-sinter" scan is to first scan the layer with half the power followed by a second scan with full power. The "overlap" strategy was where each layer was scanned twice with the second scan melting the overlap between each two adjacent melt pools.

The test specimens were cross-sectioned, mounted, and polished. Post polishing, the samples were etched using Keller's etchant [18] for microstructural examination using optical and electron microscopy. The relative density of each of the built samples was determined by image processing of three cross-sectional optical micrographs using the open source software ImageJ 1.46r. EDX was also carried out to determine the chemical composition of the built parts to determine whether some elements were more vulnerable to being lost or scattered. For a comprehensive understanding of the chemical composition and its evolution from the powder phase to the bulk phase, four types of samples were studied. These were fresh powder, recycled powder, bulk sample (processed using 50 μm hatch spacing and 250 mm/s with a single scan), as well as the debris that are scattered around the sample as a result of the laser beam–powder interaction. The debris was collected by sieving the powder left over after the SLM process.

3. Results and discussion

3.1. Powders characterization

The particle size distribution in Fig. 2 shows that the size distribution is positively skewed. The chemical composition of the alloy (see Fig. 2(b)) is found to be within the standard range. In Fig. 3(a) the particles are observed to be irregularly shaped and elongated rather than being spherical. This morphology is expected to negatively affect the process of SLM

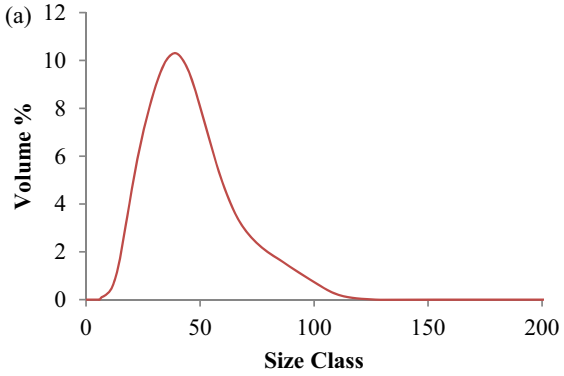

(b)

Mg	Al	Si
0.48	88.85	10.67

Fig. 2. (a) Particle size distribution and (b) chemical composition in relative weight% of LPW AlSi10Mg powders.

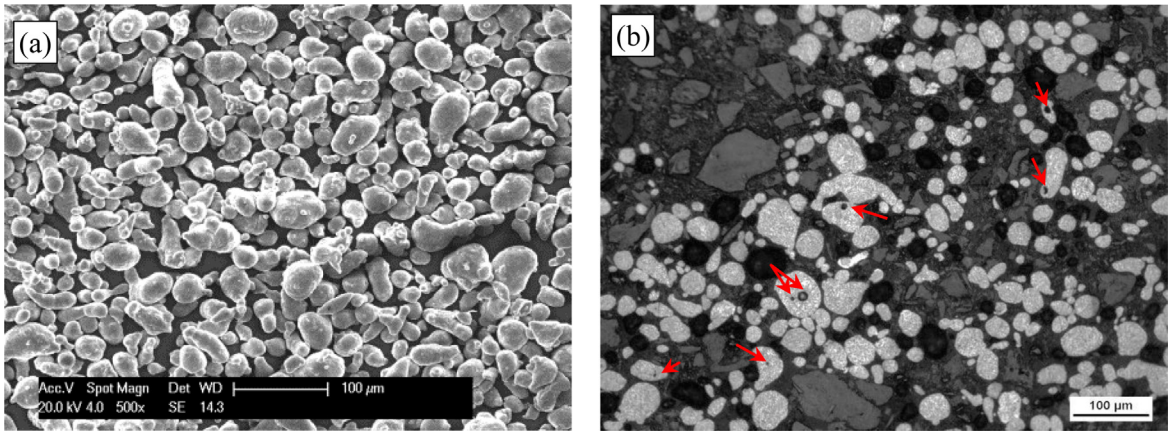

Fig. 3. (a) Morphology of LPW powder and (b) mounted cross-sectioned particles with the arrows pointing to inherent pores.

since it is favoured neither for efficient powder packing nor for flowability. Hence, the deposition of a uniform layer of powder would be poor. Also the skewed particle size distribution could be attributed to this morphology. The cross-sectioned particles revealed the internal structure of the powder (see Fig. 3(b)), which suggests the presence of trapped gases that might contribute to porosity in the bulk samples to be produced.

3.2. Hatch spacing study

When hatch spacing reached 150 µm, gaps were observed between adjacent scan tracks as seen on the top surface of polished samples and in cross-sections. They were represented as pockets of non-molten powder that was removed during grinding and polishing. The subsequent increase in porosity with increasing the hatch spacing is demonstrated in Fig. 4, along with the

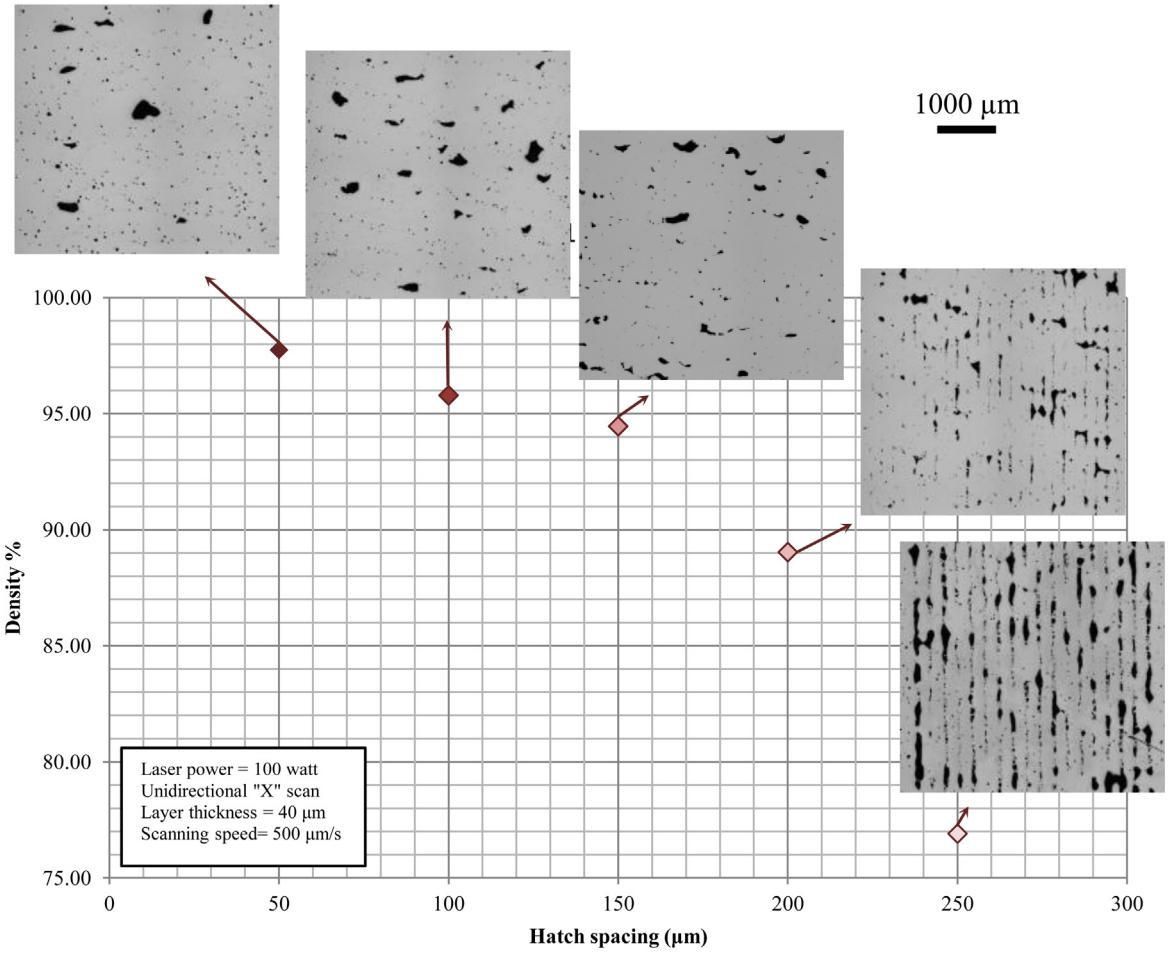

Fig. 4. Effect of changing the hatch spacing on the relative density/porosity.

Table 3
Relative density values (%) at different combinations of hatch spacing and scanning speed.

Hatch spacing (μm)	Scanning speed (mm/s)			
	250	500	750	1000
50	95.6 ± 1.8	97.7 ± 0.2	96.8 ± 1.6	96.9 ± 1.8
100	96.3 ± 0.6	95.8 ± 1.0	97.4 ± 1.4	96.3 ± 2.7

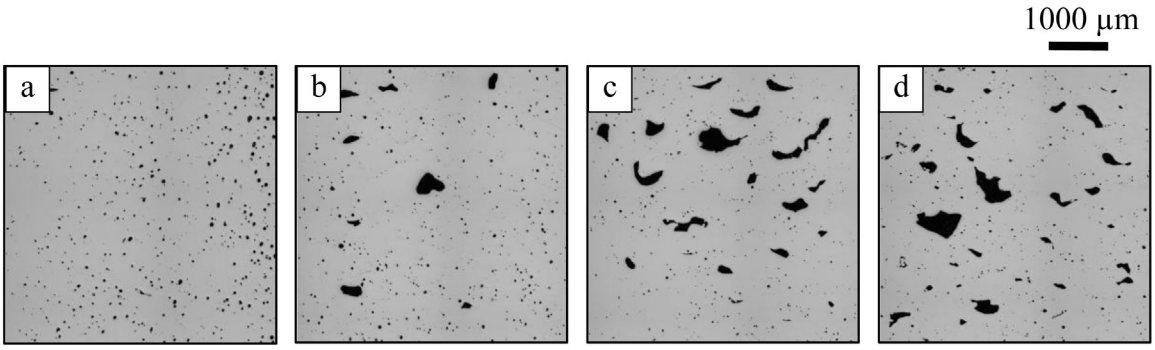

Fig. 5. Evolution of pores with scanning speed: (a) 250 mm/s, (b) 500 mm/s, (c) 750 mm/s, and (d) 1000 mm/s.

insets showing the increase in the fraction of gaps created with the hatch spacing. The gaps are formed due to lack of overlap between the scan tracks. When the hatch spacing increases, the intra-layer overlap diminishes and the part is held together mainly through interlayer bonding. Although building with large hatch spacings is a means for faster fabrication, it should be noted that larger hatch spacings will require smaller layer thicknesses to ensure both inter-layer and intra-layer overlap given the cylindrical or segmental shape of the individual melt pools, i.e. the parts will be sliced into extra number of layers, and hence further time is added [19]. A compromise between the energy density and the speed of fabrication should be considered. It was

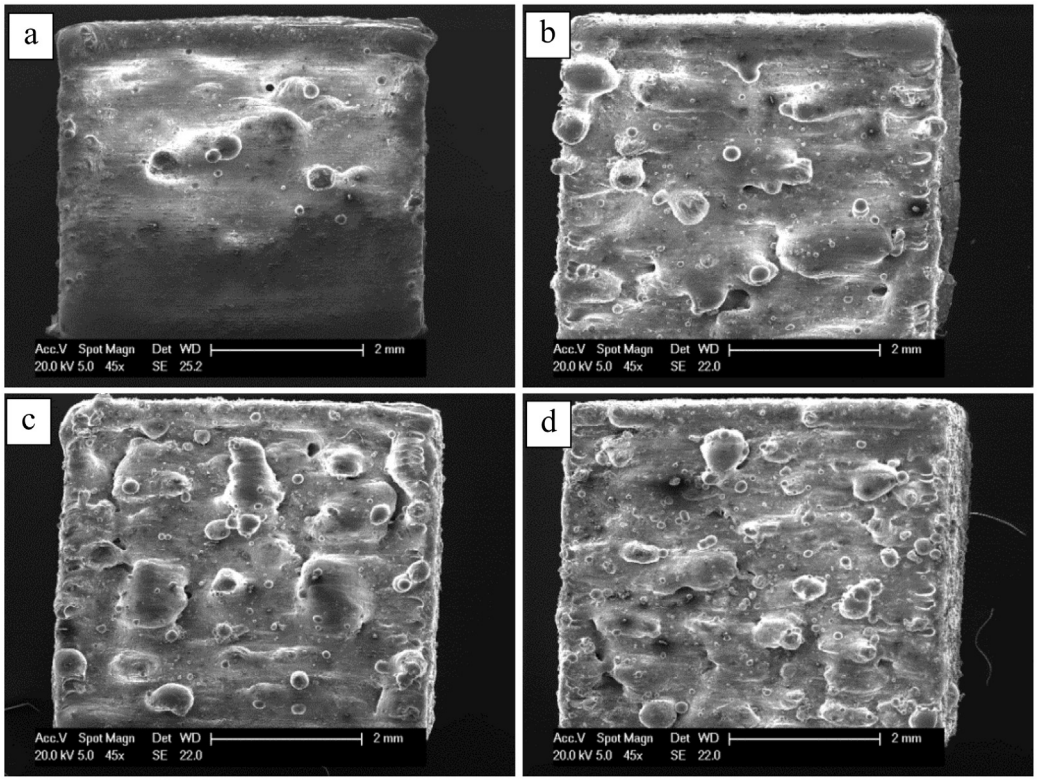

Fig. 6. Balling increase with higher scanning speeds.

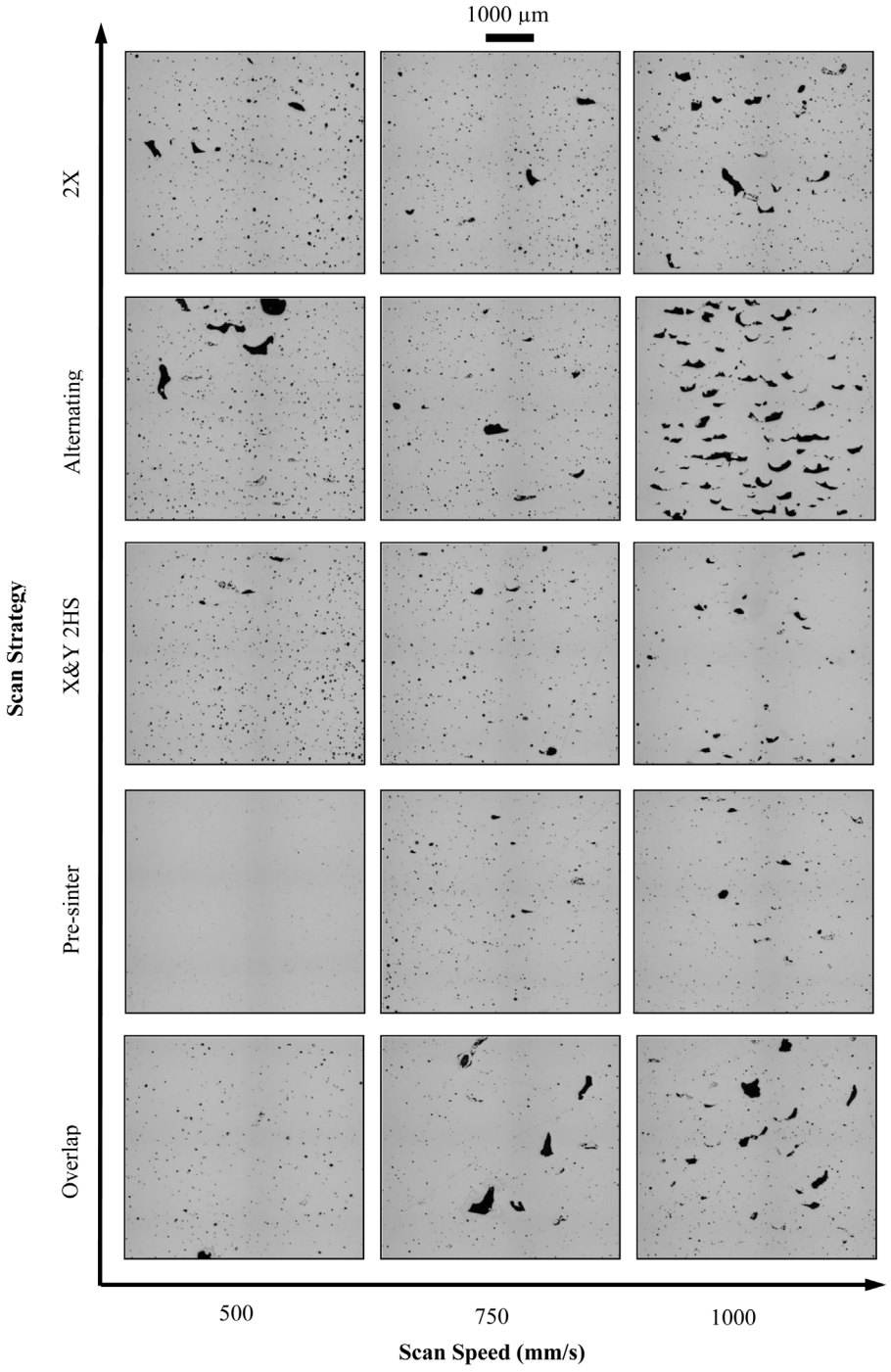

Fig. 7. Porosity evolution in AlSi10Mg samples processed using different combinations of scan speeds and scan strategies.

concluded that the best overlap was achieved when using hatch spacing values of 50 and 100 μm. Consequently, these were the values carried forward to the scanning speed study.

3.3. Scanning speed study

The average relative density values for each combination of scanning speed and hatch spacing are listed in Table 3.

The difference in relative density between using a hatch spacing of 50 μm or 100 μm for the same speed was not significant since both yield sufficient overlap between the scan tracks as established in the hatch spacing study. All the samples showed porosity between 2 and 5%. However, porosity by itself does not tell the whole story. Porosity could be categorized as metallurgical pores and keyhole pores. Metallurgical pores, also known as hydrogen porosity, are spherically shaped and small in size (less than 100 μm), whereas keyhole pores are irregularly shaped and large in size (above 100 μm) [20–22]. Metallurgical pores are created at slow scanning speeds from gases trapped within the melt pool or evolved from the powder during consolidation.

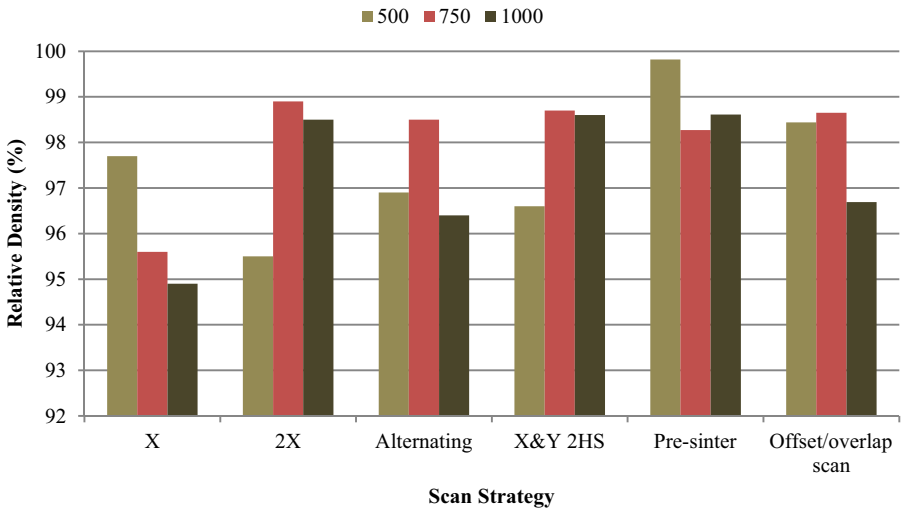

Fig. 8. Influence of scanning strategy on relative density.

Keyhole pores arise from keyhole instability, which can be attributed to rapid solidification of the metal without complete filling of gaps with molten metal [20,21]. The optical micrographs in Fig. 5 show that numerous metallurgical pores exist in samples built using a scanning speed of 250 mm/s but this number decreases with increasing the scan speed; whereas keyhole pores start to form at 500 mm/s and beyond. Thus two samples could have the same amount of porosity but caused by different types of pores. For example, scanning speeds of 250 mm/s and 1000 mm. Both show porosity in the range of 5%. Nevertheless, the 250 mm/s porosity is made up only of metallurgical pores whereas in the case of the 1000 mm/s a majority of keyhole pores are observed as seen in Fig. 5. The extensive existence of metallurgical pores at low speeds (also below 250 mm/s) could be attributed to the high energy density induced in the material.

Balling was observed on the top surface of the samples with increasing scanning speeds as evident in Fig. 6 because the high speed promotes capillary instability in the molten metal pool leading to the splashing of small liquid droplets on the surface [6]. As pointed out by Osakada et al. [1] these balls are formed due to non-linear solidification. Excessive balling results in an irregular surface and hence improper deposition of the following layer and inhomogenity in the layer, i.e. various regions having different melting and solidifying behaviours.

3.4. Scan orientation study

The effect of changing the scanning strategy on porosity can be seen in the optical micrographs in Fig. 7. At a scanning speed of 500 mm/s, scanning each layer twice was effective in reducing the keyhole pores but pores still existed when scanning the layer once in alternating scan. In the case of the overlap scan, the keyhole pores were reduced but not eliminated. The double scan per layer, whether in the form of 2X, X&Y 2HS, pre-sinter, or overlap significantly reduces (if not eliminates) the keyhole pores at all scanning speeds. However, the excessive energy leads to the extensive formation of metallurgical pores at slower speeds, i.e. the elimination of keyhole pores was at the expense of introducing metallurgical ones. At a speed of 750 mm/s, the largest fraction of keyhole pores was observed for samples with the X scan strategy (Fig. 5(c)), but they were drastically reduced by changing the scan strategy as seen in Fig. 7. Unlike the samples produced using a speed of 500 mm/s, the metallurgical pores were not significant with the double scans at this speed due to the lower energy density. Similar observations were evident for the 1000 mm/s scan speed as seen in Fig. 7.

The quantified relative density of the various samples, as shown in Fig. 8, can be seen to agree with the observations above. Starting with a highest average relative density of 97.74% using

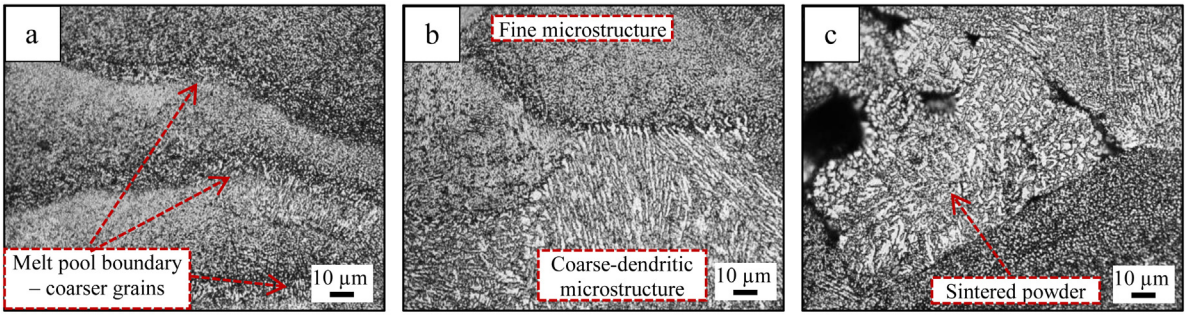

Fig. 9. Microstructure of etched samples: (a) adjacent melt pools, (b) vicinity of a keyhole pore, and (c) keyhole pore enclosing non-molten powders.

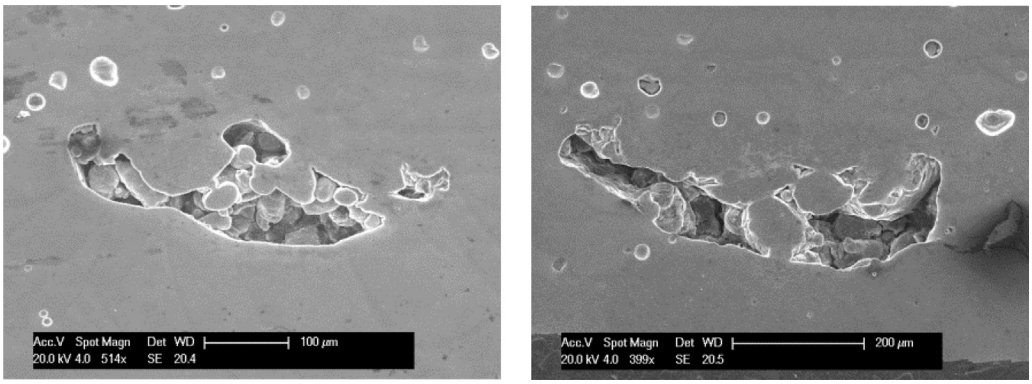

Fig. 10. Keyhole pore enclosing non-molten powders.

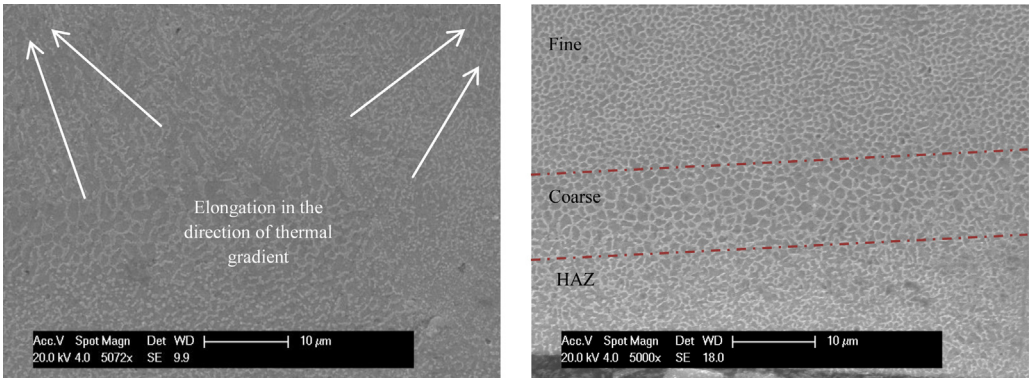

Fig. 11. Microstructure of the melt pools demonstrating grain orientation and morphology.

a 500 mm/s speed with a single unidirectional scan, the scanning strategy study has shown that a relative density of 99.82% can be achieved using a double unidirectional scan with different laser powers for the two scans (pre-sinter) at the same speed.

3.5. Microstructural analysis

The sectioned, polished, and etched samples revealed that there are two different forms of grain structure in the SLM samples, as demonstrated in Fig. 9(a). The core of the melt pool is characterized with a fine microstructure, whereas moving towards the melt pool boundary, the grains become coarser and elongated rather than equiaxed. This coarsening is due to the longer time the region stays at high temperature since being at the overlap of two adjacent melt pools results in a slower solidification rate. A coarse-dendritic microstructure was observed in the vicinity of keyhole pores (Fig. 9(b)). This is attributed to the difference between the thermal conductivity of air trapped in the keyhole pore and that of the solid material. The keyhole pores were found to contain powder that was not fully melted as shown in Fig. 9(c).

3.6. Scanning electron microscopy

Using scanning electron microscopy it was seen that the keyhole pores contained powder/particles (Fig. 10). This indicates incomplete melting of the particles at these points leading to agglomeration of powder. These defects contribute to depressing the density of the part produced. Fig. 11 shows the orientation of the grains to be elongated and pointing towards the centre of the melt pool (i.e. the heat source) because of solidification in the direction of the thermal gradient. Also it is illustrated that the melt pool is comprised of fine and coarse grains in addition to heat affected zones (HAZ), an observation previously reported by Thijs et al. [2]. The fine microstructure is at the core of the melt pool, this then starts to coarsen moving farther from the centre-line, since this represents the overlap region of two neighbouring melt pools, until reaching the heat affected zone at the borders.

3.7. Energy dispersive spectroscopy

Comparison of the chemical composition of the fresh and recycled powder (Table 4) suggests that the use of recycled powder would not be expected to negatively affect the quality of the produced samples. It can also be seen in Table 4 that there is a

Table 4
Chemical composition of powders and bulk sample in relative weight%.

Sample	Al	Si	Mg
Fresh powders	88.85	10.67	0.48
Recycled powders	88.60	10.90	0.49
Bulk sample	89.37	10.35	0.28
Debris	85.8	13.00	1.10

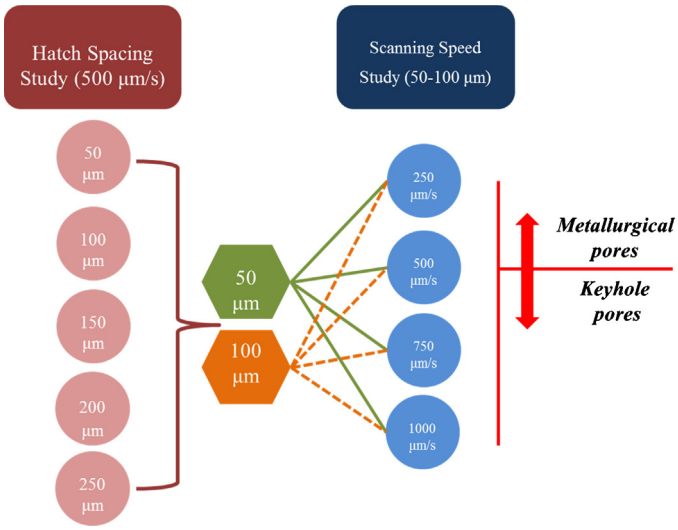

Fig. 12. Summary of the study and findings.

significant difference between the chemical composition of the bulk sample and the fresh powder as the amount of Mg in the bulk has dropped to almost half its original value. This could be due to the evaporation of Mg during the SLM process since it is the lightest element in the alloy as a response to the high energy density induced in the sample by using a small hatch spacing (50 µm) and a slow scan speed (250 mm/s). There is also a slight decrease in the amount of Si in the bulk sample. This finding agrees well with the chemical composition of the debris which can be seen to be rich in both Mg and Si when compared to the fresh powder.

4. Summary and conclusions

The study conducted is summarized in the schematic diagram in Fig. 12. First, sufficient overlap between adjacent melt pools was achieved at 50 and 100 µm hatch spacing. As indicated by Pupo et al. [23], heat accumulation in the melt pool occurs when using smaller hatch spacings since it allows slow cooling of the layer giving a homogeneous and continuous layer. Consequently, it is recommended to use the smaller hatch spacing. Second, based on these hatch spacings the effect of the scanning speed was investigated. This study showed that the type of pore formed during the process of SLM is related to the scanning speed used, metallurgical pores tend to be formed at lower speeds whereas keyhole pores are created with increasing scanning speed, along with a reduction in metallurgical pores. The bordering speed is 500 mm/s.

Keyhole pores enclose non-molten powder and their formation is parameter-dependent. Irregularities on the surface, such as balling, that occur with increasing scan speed promote the capture of powder that is not fully melted by the laser beam scanning the following layer; hence a keyhole pore is created. This scenario is supported by the effect of altering the scan strategy since scanning the same layer twice has resolved this issue specially using the pre-sinter scan strategy that flattens the surface before the second scan. Altering the scan strategy to a double scan at high speeds was an alternative to solely reducing the scanning speed in pursuit of keyhole pore prevention, as the latter introduces metallurgical pores. Some metallurgical pores were still seen at high speeds but it is worth noting that a fraction of the pores (metallurgical) could be inherent porosity in the powder. Surveying the windows of parameters, the best combination was found to be a speed of 500 mm/s, hatch spacing 50 µm, and 100 W laser power when using a layer thickness of 40 µm and employing the pre-sinter scan strategy yielding a relative density of $99.77 \pm 0.08\%$. It is worth noting that the achieved relative density using a 100 W only laser power is high compared to the values reported in the literature where similar densities were achieved using a minimum of 200 W laser power, such as the work by Thijs et al. [2].

Two categories of microstructure are created in the melt pool; the first was a fine microstructure at the centre of the melt pool and the second was a coarse structure at the melt pool boundary. The grains were seen to be elongated in the direction of the thermal gradient, i.e. the heat source. Moreover, coarse dendritic structures were formed in the vicinity of keyhole pores.

Magnesium, as the lightest element in the studied alloy, had a higher susceptibility to evaporation or scatter resulting in the production of parts with reduced Mg content compared to the raw virgin powder; this was confirmed by the excess amount of Mg found in the debris. Although Mg as an element does not affect the melting and solidification behaviour of the material, the effect of this change in composition on precipitate formation and consequently mechanical properties needs further investigation.

Acknowledgments

Nesma T. Aboulkhair gratefully acknowledges funding provided by the Dean of Engineering Scholarship for International Research Excellence, Faculty of Engineering, University of Nottingham, United Kingdom.

References

[1] Osakada K, Shiomi M. Flexible manufacturing of metallic products by selective laser melting of powder. Int J Mach Tool Manuf 2006;46:1183–93.
[2] Thijs L, Kempen K, Kruth J-P, Van Humbeeck J. Fine-structured aluminium products with controllable texture by selective laser melting of pre-alloyed AlSi10Mg powder. Acta Mater 2013;61:1809–19.
[3] Kempen K, Thijs L, Van Humbeeck J, Kruth JP. Mechanical properties of AlSi10Mg produced by selective laser melting. Phys Procedia 2012;39:439–46.
[4] Bartkowiak K, Ullrich S, Frick T, Schmidt M. New developments of laser processing aluminium alloys via additive manufacturing technique. Phys Procedia 2011;12 Part A:393–401.
[5] Buchbinder D, Schleifenbaum H, Heidrich S, Meiners W, Bültmann J. High power selective laser melting (HP SLM) of aluminum parts. Phys Procedia 2011;12 Part A:271–8.
[6] Zhang B, Liao H, Coddet C. Effects of processing parameters on properties of selective laser melting Mg–9% Al powder mixture. Mater Design 2012;34:753–8.
[7] Louvis E, Fox P, Sutcliffe CJ. Selective laser melting of aluminium components. J Mater Process Technol 2011;211:275–84.
[8] Gibson I, Rosen DW, Stucker B. Additive manufacturing technologies. New York, USA: Springer; 2010.

[9] Kempen K, Thijs L, Yasa E, Badrossamay M, Verheecke W, Kruth J-P. Process optimization and microstructural analysis for selective laser melting of AlSi10Mg; 2011. Available at: http://utwired.engr.utexas.edu/lff/symposium/proceedingsArchive/pubs/Manuscripts/2011/2011-37-Kempen.pdf [accessed May 2014].
[10] ASTM Standard B213-13. Standard test methods for flow rate of metal powders using the hall flowmeter funnel. West Conshohocken, PA: ASTM International; 2013, http://dx.doi.org/10.1520/B0213-13 www.astm.org
[11] Boivineau M, Cagran C, Doytier D, Eyraud V, Nadal MH, Wilthan B, et al. Thermophysical properties of solid and liquid Ti-6Al-4V (TA6V) alloy. Int J Thermophys 2006;27:507–29.
[12] Material properties handbook: titanium alloys. United States of America: ASM International; 1994.
[13] ASM metals reference book. 3rd ed. United States of America: ASM International; 1993.
[14] Schreuder D. Outdoor lighting: physics, vision and perception. New York, USA: Springer; 2008.
[15] Macleod HA. Thin film optical filters. 3rd ed. United Kingdom: CRC Press; 2001.
[16] Olakanmi EO. Selective laser sintering/melting (SLS/SLM) of pure Al, Al–Mg, and Al–Si powders: effect of processing conditions and powder properties. J Mater Process Technol 2013;213:1387–405.
[17] http://www.malvern.com/en/products/product-range/mastersizer-range/mastersizer-3000/ [accessed May 2014].
[18] Voort GFV. Metallography: principles & practice. United States of America: ASM International; 1999.
[19] Su X, Yang Y. Research on track overlapping during selective laser melting of powders. J Mater Process Technol 2012;212:2074–9.
[20] Dahotre NB, Harimkar S. Laser fabrication and machining of materials. New York, USA: Springer; 2008.
[21] Xiao R, Zhang X. Problems and issues in laser beam welding of aluminum–lithium alloys. J Manuf Process 2014;16:166–75.
[22] Haboudou A, Peyre P, Vannes AB, Peix G. Reduction of porosity content generated during Nd:YAG laser welding of A356 and AA5083 aluminium alloys. Mater Sci Eng A 2003;363:40–52.
[23] Pupo Y, Delgado J, Serenó L, Ciurana J. Scanning space analysis in selective laser melting for CoCrMo powder. Procedia Eng 2013;63:370–8.